

APPLICATION OF FLUORESCENT PIV AND DIGITAL IMAGE ANALYSIS TO MEASURE TURBULENCE PROPERTIES OF SOLID-LIQUID STIRRED SUSPENSIONS

H. Unadkat*, C. D. Rielly, G. K. Hargrave and Z. K. Nagy

* Dept. of Chemical Engineering, Loughborough University, Loughborough, Leicestershire, LE11 3TU, UK; e-mail: H.Unadkat@lboro.ac.uk

Abstract. This study describes an experimental technique which combines Fluorescent Particle Image Velocimetry (FPIV) and digital image analysis, to quantify the hydrodynamics of a solid-liquid suspension stirred by a 45° pitched-blade turbine impeller. Soda-lime glass spheres of 1000 µm diameter were employed for the dispersed phase, with up to volumetric concentrations of 0.5 vol% in water. The magnitude of the continuous phase mean velocity did not change significantly in the impeller jet or bulk flow, with the addition of up to 0.5 vol% dispersed phase. Turbulence levels of the continuous phase, in terms of rms velocities, turbulent kinetic energy and dissipation rate decreased.

Key words: Mixing, Multiphase flows; Turbulence; Particle Image Velocimetry; Phase separation

1. INTRODUCTION

Solid-liquid suspensions are found in a wide variety of stirred tank applications such as solid-catalyzed reactions, dissolution and crystal growth. These processes may involve micro-mixing or mass transfer, which strongly depend on the system turbulence. The presence of the dispersed phase modulates the turbulent environment; previous studies of multiphase flows in geometries other than stirred vessels, have reported up to 50% turbulence damping by small particles, and up to 360% increase by larger particles [1]. It has been suggested that this transition occurs when the particle diameter to characteristic fluid length-scale ratio is 0.1. Other theories have also been postulated to relate these effects to the particle Reynolds number and wake shedding [2]. Knowledge of the hydrodynamics of stirred suspensions may enable optimization of the system geometry as well as operating conditions, which may improve, for instance, the yield of a product in a solid-catalysed reaction.

Although solid-liquid stirred flows are a common unit operation, there is a lack of reliable and detailed experimental data regarding these systems, mainly due to limitations of previously available measurement techniques. This has held back the validation of predictive two-phase models, which should include inter-phase turbulence transfer terms for turbulence modulation. In the absence of such information, most models employ extensions of the standard single-phase $k-\epsilon$ model [3]. For instance, the homogeneous $k-\epsilon$ model assumes that both solid and liquid phases share the same turbulent kinetic energy and dissipation rate.

Particle Image Velocimetry (PIV) techniques are traditionally used to visualise single phase flows, to determine information regarding their fluid velocities and turbulence levels. The opacity of most multiphase systems and increased interphase noise limits the application to study solid suspensions at elevated concentrations. However, with the inclusion of

refractive index (RI) matching, optical filtering and digital post processing, some of these challenges may be overcome. The authors are aware of only one other study which has attempted to characterise turbulence modulation in solid-liquid stirred suspensions using PIV, with up to 1.5 vol% solid concentration [4]. The current paper presents a combination of fluorescent PIV (FPIV) and digital image analysis techniques for simultaneous velocity measurements of both phases in a stirred flow. The influence of concentration on turbulence properties such as rms velocity, turbulence kinetic energy (k) and dissipation rate (ϵ) will be quantified for experiments with up to 0.5 vol% of 1000 μm dispersed particles.

2. EXPERIMENTAL SETUP

Experiments were carried out in a baffled stirred tank of diameter $T = 101$ mm, equipped with a 45° pitched-blade turbine of diameter $D = T/3$, which operated at a clearance of $C = T/4$ from the vessel base. The four baffles had a width equal to $T/10$. The tank was filled to a height $H = T$ with water. The vessel was placed inside a square tank also filled with water, to limit optical distortion at the curved surface. The vessel was made of cylindrical glass; all other components were made of acrylic glass. The dispersed phase particles were 1000 μm solid soda-lime glass beads of density 2500 kg m^{-3} and RI 1.51 at the Sodium D-line ($\lambda = 589.3$ nm) at 20°C . Experiments were initiated with particles suspended in the fluid at a volumetric concentration of 0.01 vol%, and increased incrementally until the laser light sheet extinction was too severe to enable further PIV measurements to be taken. This limit was found to be 0.5 vol%.

Fluorescent tracer particles of diameter 30 μm , doped with Pyrromethene 597-8C9 dye (exciton) were manufactured in the laboratory from Polystyrene (PS) cross-linked with divinyl benzene (DVB), and used to seed the water. The dye has an absorption peak at 527.8 nm (close to the laser excitation wavelength of 532 nm), and a fluorescence peak at 590 nm in diesel fuel. The Pyrromethene dyes are not very solvo-chromatic, hence the wavelength changes would be small (5 to 10 nm at most) in the PS/DVB material.

The measurement technique involved a combination of fluorescence tagging and digital image treatment. The experimental setup is depicted in Fig. 1. The system employed a two-camera PIV setup. One camera was fitted with two long-pass Schott OG550 filters (UQG Ltd) with a cut-off at 550 nm, which transmitted fluorescence at higher wavelengths. In this way, the camera captured images of the fluorescent tracers without interphase noise, which could be processed to obtain velocity fields without any further treatment. PIV analysis was conducted using cross-correlation techniques with interrogation area (IA) sizes of 32×32 pixels, with 50% overlap. The particle diameter (1 μm) was comparable to the IA spatial resolution. However, the majority of particles appeared as two ‘half moon’ shapes rather than filled circles in the images. They did not always occupy the entire IA and enabled enough fluorescence from the tracers to be transmitted for cross-correlation. In cases where particles overlapped or where particles saturated the IA , no additional measures were taken to avoid the problem of insufficient seeding. Instead, the cross-correlation signal peak-to-noise ratio was set relatively higher than the single phase case, so that vectors from these low seeding regions would be eliminated. The holes were later filled with interpolation of the surrounding vectors.

The second camera simultaneously captured Mie scattering images of both phases on a single frame, which were digitally post-processed to extract information corresponding to the dispersed phase. The particle velocities were obtained via cross-correlation, analogous to the continuous phase, using 32×32 pixel IA s with 50% overlap.

The cameras were two 8-bit TSI PIVCAM 10-30 Model 630046 cross-correlation cameras, with a resolution of 1000×1016 pixels. The system was equipped with a double-pulsed New-Wave Nd:YAG Solo III laser of 532 nm wavelength and 50 mJ pulse energy. The laser light sheet thickness was approximately 1 mm. The image acquisition rate was 15 Hz

(for double pulses), with a pulse width of 6 ns and pulse delay of 263 μ s. The time separation between two exposures in an image pair was 50 μ s in each experiment.

Ensemble-averaged measurements were obtained in the impeller region, where the highest turbulence level was expected. The field of view was 28×28 mm² and included the blade. The baffle at the edge of the field of view was positioned just behind the laser light sheet, such that its reflections did not appear in the images. A recent study revealed that the mean flow and turbulence properties can be characterised using a minimum of 575 vector fields [4]. Consequently, 600 double image pairs were obtained in each evaluation, and were considered to be sufficient. In all experiments the impeller speed was set at 1600 rpm, which is above the just-suspended speed characterized by the Zwietering criterion [5], ensuring complete off-bottom suspension.

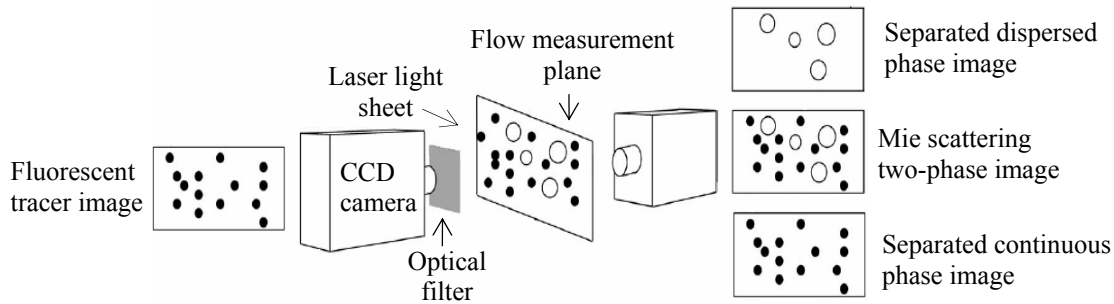


Fig. 1: Experimental setup of the two-camera FPIV system

3. IMAGE ANALYSIS

After reviewing various phase separation techniques in literature, it was decided to process the multiphase Mie scattering images by the application of an algorithm based on differences in geometrical characteristics of the particles. The ‘two-parameter phase discrimination technique’ was believed to be the best choice, since it considered differences in both particle size and intensity simultaneously [6]. The object detection and particle centroid location stages of the algorithm were adapted to fit the current study, due to observed differences in the image patterns of the dispersed phase particles. The various steps of the algorithm are described below.

3.1 Object detection

In the original study [6], the authors employed second order intensity gradients to identify objects within the images. This was based on the consideration that the intensity I reaches a maximum in a two-dimensional image of both tracers and solid particles. In order to be able to identify each maximum however, it is necessary to capture circular images, and the intensity distribution within these regions must be smooth and approximately Gaussian. In the present experiments, dispersed particle clusters, broken particles, and particles at the edge of the light sheet did not appear to be circular. Moreover, the dispersed particles manifested themselves as two adjacent ‘half moon’ shapes in the images rather than circles, due to the refraction of light at the edges of the particles. In these cases, the dispersed particles would not be picked up using second-order spatial derivatives. An alternative routine was developed and implemented in Matlab. Firstly, the background was extracted by performing a ‘morphological opening operation’ which removes objects that do not saturate a given structuring element, created using the *strel* function. The background was then subtracted from the images to make them more uniform. Next the image contrast was adjusted, and the gray scale images were binarized into black and white form via thresholding. Finally, all objects were detected using the *bwlabel* function in the Matlab image processing toolbox.

3.2 Parameterization

All detected objects were assigned the parameters of size (in pixels) and average gray-scale intensity (or brightness) [6]. Subsequently, a contour plot of total signal versus size and brightness was constructed. The total amount of signal carried by objects with a given combination of size and brightness was calculated as $size \times brightness \times number\ density$, where number density is the number of objects with a given size and brightness. A sample size-brightness map is shown in Fig. 2.

3.3 Phase separation

As may be observed in Fig. 2, the size-brightness map displays two regions containing signals carried by the dispersed particles and tracers. Separation limits (i.e. the size and brightness characterizing each phase) were obtained by defining two non-overlapping rectangles, which contained the strongest signals within each region. This ensured that a cluster of bright tracers would not be mistaken for dispersed particles, and that small dim particles would not be mistaken for tracers. Data which fell outside of these limits were discarded.

It may be observed that the signal from the tracers yields a distinct peak, since there are a large number of them in the images. Fewer dispersed particles generate scattered data points; however the majority of them can still be confined within a boundary. Subsequently, all objects falling within the region occupying the dispersed phase separation limit were treated as dispersed solids. Their corresponding pixel and gray-scale intensity information was extracted from the raw data and placed on a black background, forming ‘separated dispersed phase’ images.

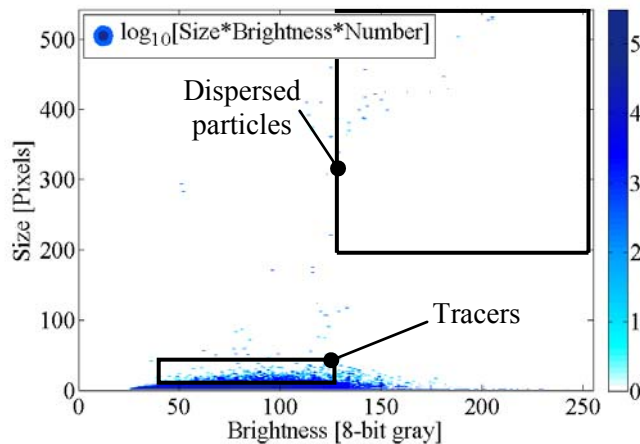


Fig. 2 : Sample size-brightness map of a real two-phase Mie-scattering PIV image

4. RESULTS AND DISCUSSIONS

The results of single and continuous phase stirred flows with 1000 μm dispersed particles up to 0.5 vol% are shown in this section. From Fig. 3 it appears that the mean velocities of the continuous phase do not change significantly in the impeller suction or jet, with the incorporation of 1000 μm particles at 0.5 vol%. This is in contrast to a previous study [8] which reported a decrease in the impeller discharge flow rate and wall jet velocity, due to the effects of particle inertia and gravity, respectively. Another study [4] has also reported a decrease in the axial velocity of around 70% at a solid concentration of 1.5 vol%. It may be observed that the vortex close to the tank wall has moved 3 mm away from the wall in the flow containing 0.5 vol% particles, relative to the single phase case; the vortex centres (or zero velocity regions) are marked in Fig. 3 to show this more clearly. This trend was observed for experiments carried out with volume fractions above 0.2 vol% (but not at the lower

volume fractions). For this reason, the axial velocity profile in Fig. 4(a) depicts a change in direction of the axial flow from downwards to upwards at $r/T = 0.32$ in the wall jet, for > 0.2 vol% dispersed phase. In Fig. 4(b) it can be seen that the magnitude of the mean radial velocities also appear to be increased by 50% close to the tank wall above 0.2 vol% dispersed phase. This result is not a real increase in the wall jet velocity, but an artefact due to the shift of the centre of the flow circulation loop.

The turbulent kinetic energy was calculated using a pseudo-isotropic assumption, as given by eq.(1), where u' and v' are the radial and axial fluctuating velocity components respectively. The overbar represents an average taken over the data set comprising 600 vector fields. Note that the axial and radial rms contour plots in Figs 5 and 6 illustrate anisotropy of the flow; however with 2-D PIV measurements there is no tangential velocity component, and hence eq.(1) was used out of necessity.

$$k = \frac{3}{4}(\overline{u'^2} + \overline{v'^2}) \quad (1)$$

The superimposed turbulent kinetic energy (TKE) plots in Fig. 3 indicate turbulence damping in the impeller jet after the addition of 0.5 vol% dispersed phase. This is further reflected in the axial and radial rms velocity contour plots in Figs 5 and 6. Specifically, the maximum radial rms velocity decreased by 7%, and the maximum axial rms velocity by 12.5%; both were in the impeller jet. In addition to the points of maxima, the turbulence levels in the impeller jet have also reduced in magnitude, although they remain unaffected in the bulk of the flow. This result is different to an earlier study [8], which found that the rms axial and radial velocity of the fluid was unaffected by the presence of 253 μm dispersed particles at 0.5 vol%. On the other hand, a more recent and similar study [4] has reported an increase in the rms level, also at 0.5 vol% for 1000 μm particles. However, one study which supports the current observation [9] has previously reported turbulence suppression in all regions of the tank by 50% when dispersing 186 μm particles at 0.5 vol%. The last two mentioned studies reported corresponding particle diameter to characteristic fluid length scale ratios of 0.14-0.66 [4] and 0.15 [9] respectively.

The dissipation rate was calculated using the 2-D LES analogy [10], which was found to be the best method compared to dimensional analyses and the direct estimate (due to spatial resolution limitations). In LES, the Navier-Stokes (NS) equations are solved directly for the large scales, whereas the small scales are modelled via sub-grid-scale (SGS) models. The spatial resolution of PIV measurements usually exceeds the smallest eddy sizes that govern the dissipation rate. Thus, by adopting the LES analogy, it is possible to measure the resolved velocity field (analogous to solving the NS equations), and then model the unresolved scales via a SGS model. The interrogation area size is naturally the spatial filter. The Reynolds averaged SGS dissipation rate (ε_{SGS}) is given by:

$$\varepsilon \approx \overline{\varepsilon_{SGS}} = -2\overline{\tau_{ij}s_{ij}}, \quad (2)$$

where s_{ij} is the resolved scale strain rate tensor calculated from gradients of the instantaneous resolved scale velocity fields:

$$s_{ij} = \frac{1}{2} \left(\frac{\partial u_j}{\partial x_i} + \frac{\partial u_i}{\partial x_j} \right) \quad (3)$$

and τ_{ij} is the SGS stress tensor. The strain rate tensor consists of a total of nine components, of which five are known from PIV measurements. Subsequently, the sum of the product of the strain rate and stress tensor was multiplied by a factor of 9/5. Note that when statistical isotropy assumptions were employed to calculate the unknown gradients terms, the maximum

dissipation rate estimate was $\sim 17\%$ greater than that obtained from scaling the strain rate tensor components, although the spatial distribution remained unchanged.

Fig. 7 illustrates a clear decrease in the local dissipation rate after the addition of 0.5 vol% of 1000 μm diameter particles. The maximum dissipation rate has decreased by $\sim 21\%$. Similar to the rms velocities, the magnitudes in the impeller jet have decreased, whereas the dissipation rates in the bulk of the flow seem to be largely unaffected. Experiments carried out at 0.3 and 0.4 vol% showed similar trends for the TKE and dissipation rate, as depicted in Figs. 8(a) and (b).

Locally averaged particle concentration fields were obtained by the following procedure. The separated dispersed phase images were binarized and divided into small non-overlapping rectangular regions (analogous to *IAs* in cross-correlation) of size 25×25 pixels. The number of bright pixels per each region was averaged across all (600×2) images in the data set. Normalizing the result by the total number of pixels in that area (625 pixels) was equivalent to the average local volumetric concentration. The spatial distribution of the local concentration field is given in Fig. 9(a), where 100% would indicate that particles fully occupied a particular region in all image frames. It may be observed that particles are not distributed homogeneously in the fluid. Instead, there is a locally high concentration above and below the impeller region, as well as a stagnation point at the bottom of the vessel, where the base meets the wall. This suggests that the observed turbulence suppression is a genuine effect, and a direct consequence of the presence of particles in the discharge stream.

Dispersed phase velocities were also obtained via cross-correlation analyses. The mean velocity field superimposed with the TKE is shown in Fig. 9(b). The particle velocity field is much more noisier than the continuous phase, because the average is a result of fewer vectors. Points where particles never passed the field of view over the entire data set resulted in holes in the mean field. It may be observed that the TKE of the dispersed particles is less than that of the corresponding continuous phase in Fig. 3(b) by $\sim 22\%$ in the discharge stream. However, an average over more particle velocity vectors is required for a reliable estimate.

5. CONCLUSIONS

This paper presents the development of an adapted phase discrimination algorithm which has been successfully applied to study stirred suspensions of 1000 μm particles with up to 0.5 vol% dispersed phase. A commonly reported result [1] is that particles which have a diameter to characteristic fluid length scale ratio greater than $O(0.1)$ enhance turbulence. Using the 2-D integral length scale of the fluctuating axial velocity component obtained from PIV, this ratio was found to be 0.29 in the current study, which suggests turbulence augmentation. The present results show the opposite effect of turbulence suppression and hence further tests using other particle sizes will be carried out to substantiate the observations.

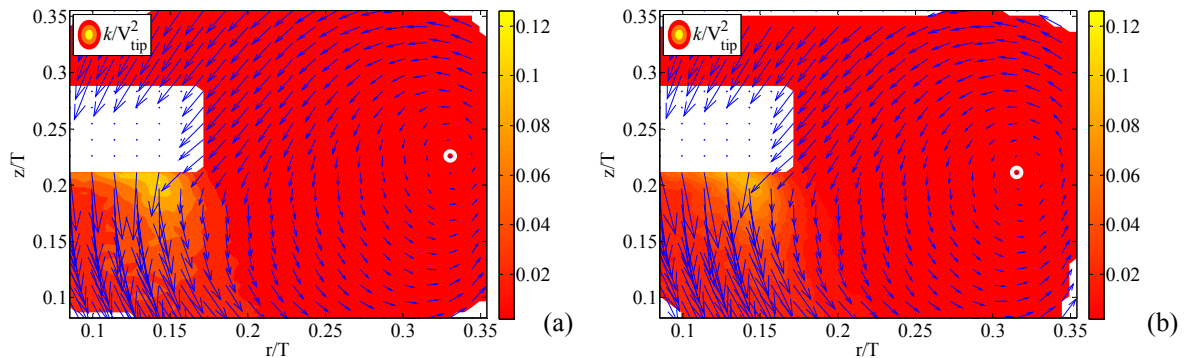


Fig. 3: Velocity (vectors) and normalized TKE (contours) of (a) single phase and (b) continuous phase stirred flow with 1000 μm 0.5 vol% dispersed particles

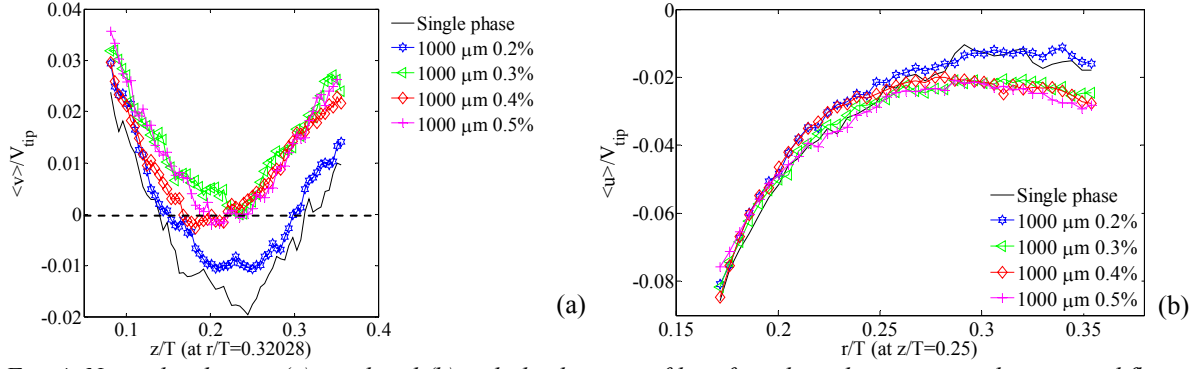


Fig. 4: Normalized mean (a) axial and (b) radial velocity profiles of single and continuous phase stirred flows with 1000 μm particles between 0.01 and 0.5 vol%

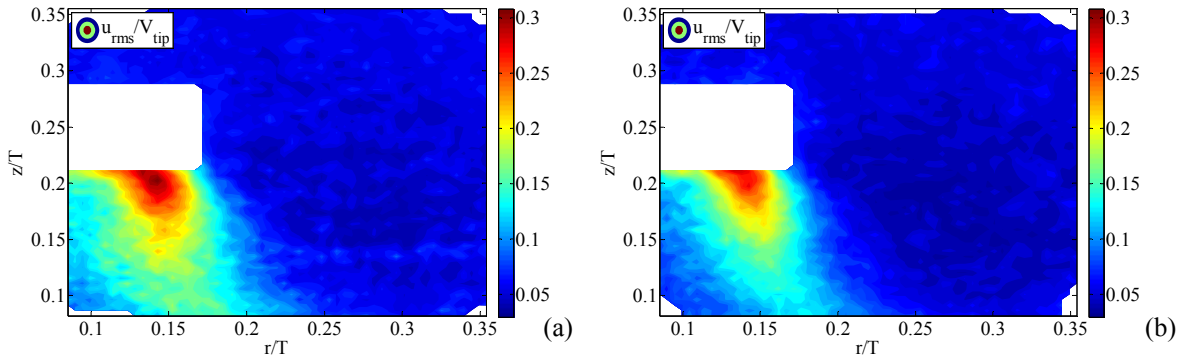


Fig. 5: Normalized radial rms velocity of (a) single phase and (b) continuous phase stirred flow with 1000 μm 0.5 vol% dispersed particles

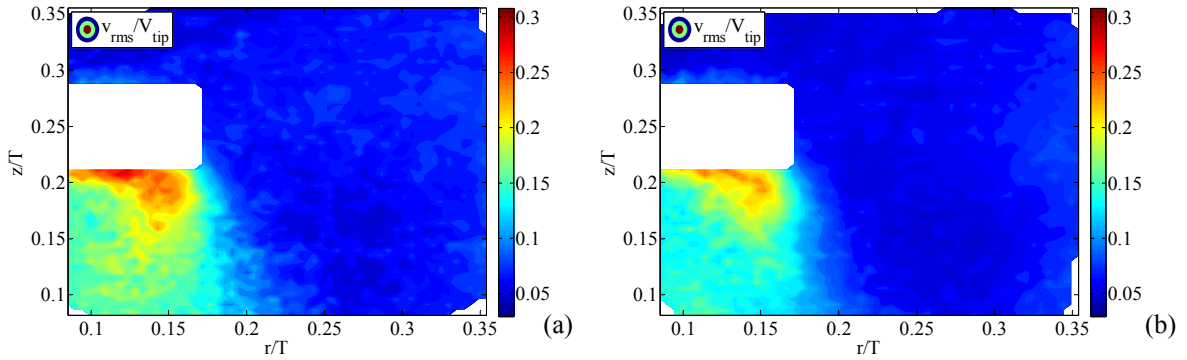


Fig. 6: Normalized axial rms velocity of (a) single phase and (b) continuous phase stirred flow with 1000 μm 0.5 vol% dispersed particles

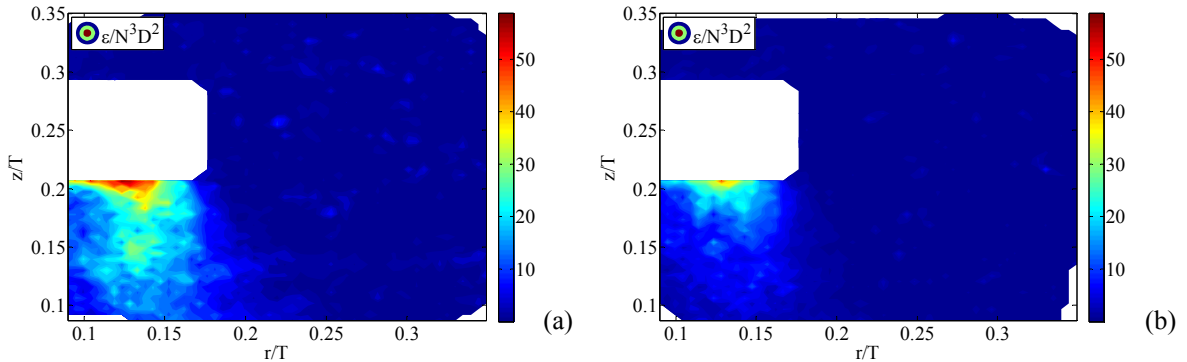


Fig. 7: Normalized dissipation rate of (a) single phase and (b) continuous phase stirred flow with 1000 μm 0.5 vol% dispersed particles

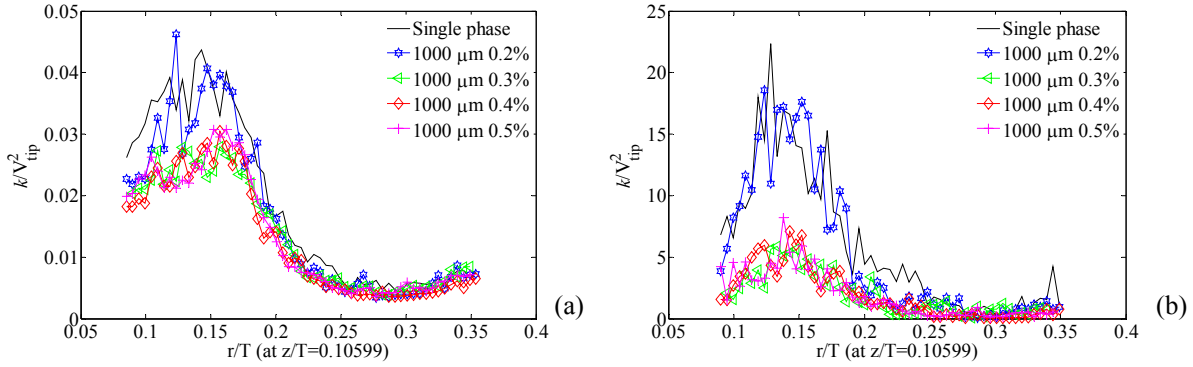


Fig. 8: Normalized (a) TKE and (b) dissipation rate profiles of single and continuous phase stirred flows with 1000 μm particles between 0.01 and 0.5 vol%

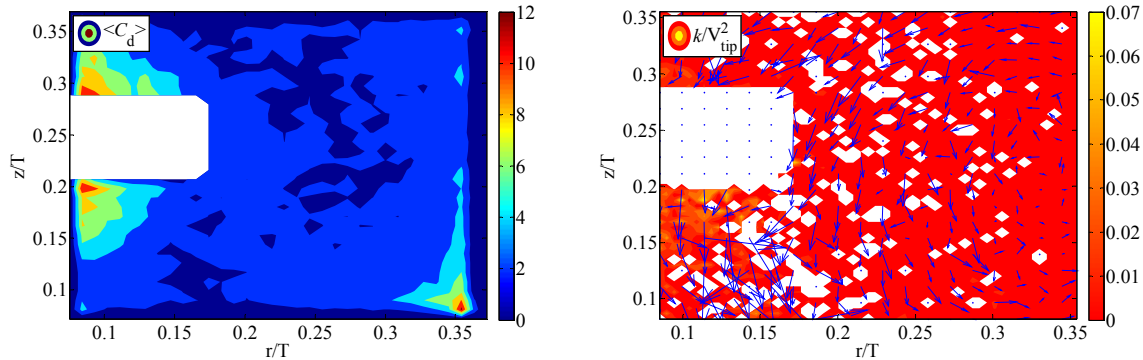


Fig. 9: (a) Locally averaged volumetric concentration field and (b) velocity (vectors) with normalized TKE (contours) of the dispersed phase, 1000 μm particles 0.5 vol%

6. REFERENCES

1. Gore R. A., Crowe C. T., (1991), "Modulation of turbulence by a dispersed phase", *J. Fluid Eng.-T. ASME*, **113**, 304-307.
2. Hetsroni G., (1989), "Particles-turbulence interaction", *Int. J. Multiphase Flow*, **15**, 735-746
3. Montante G., Magelli F., (2007), "Mixed solids distribution in stirred vessels: Experiments and computational fluid dynamics simulations", *Ind. Eng. Chem. Res.*, **46**, 2885-2891.
4. Virdung T., Rasmuson A., (2008), "PIV measurements of solid-liquid mixing at elevated concentrations", *Chem. Commun.*, **195**, 18-34.
5. Zwietering T. N., (1958), "Suspensions of solid particles in liquid by agitators", *Chem. Eng. Sci.*, **8**, 244-253.
6. Khalitov D. A., Longmire E. K., (2002), "Simultaneous two-phase PIV by two-parameter phase discrimination", *Exp. Fluids*, **32**, 252-268.
7. Hassan Y. A., Philip O. G., (1997), "A new artificial neural network tracking technique for particle image velocimetry", *Exp. Fluids*, **23**, 145-154.
8. Guiraud P., Costes J., Bertrand, J., 1997, "Local measurements of fluid and particle velocities in a stirred suspension", *Chem. Eng. J.*, **68**, 75-86
9. Micheletti M., Yianneskis, M., 2004, "Study of fluid velocity characteristics in stirred solid-liquid suspensions with a refractive index matching technique", *Proc. Instn Mech. Engrs*, **218**, 191-204.
10. Sheng J., Meng H., Fox, R. O., (2000), "A large eddy PIV method for turbulence dissipation rate estimation, *Chem. Eng. Sci.*, **55**, 4423-4434.